Title

Additional Sodium Insertion into Polyanionic Cathodes for Higher-Energy Na-Ion Batteries

Journal

Advanced Energy Materials, 7(18)

ISSN

1614-6832

Authors

Bianchini, M

Xiao, P

Wang, Y

et al.

Publication Date

2017-09-20

DOI

10.1002/aenm.201700514

Peer reviewed

Additional Sodium Insertion into Polyanionic Cathodes for Higher-Energy Na-Ion Batteries

*Matteo Bianchini, Penghao Xiao, Yan Wang, and Gerbrand Ceder**

Na-ion technology is increasingly studied as a low-cost solution for grid storage applications. Many positive electrode materials have been reported, mainly among layered oxides and polyanionic compounds. The vanadium oxy/flurophosphate solid solution $Na_3V_2(PO_4)_2F_{3-y}O_{2y}$ ($0 \le y \le 1$), in particular, has proven the ability to deliver ≈500 Wh kg^{-1}, operating on the V^{3+}/V^{4+} ($y = 0$) or V^{4+}/V^{5+} redox couples ($y = 1$). This paper reports here on a significant increase in specific energy by enabling sodium insertion into $Na_3V_2(PO_4)_2FO_2$ to reach $Na_4V_2(PO_4)_2FO_2$ upon discharge. This occurs at ≈1.6 V and increases the theoretical specific energy to 600 Wh kg^{-1}, rivaling that of several Li-ion battery cathodes. This improvement is achieved by the judicious modification of the composition either as O for F substitution, or Al for V substitution, both of which disrupt Na-ion ordering and thereby enable insertion of the 4th Na. This paper furthermore shows from operando X-Ray Diffraction (XRD) that this energy is obtained in the cycling range $Na_4V_2(PO_4)_2FO_2$–$NaV_2(PO_4)_2FO_2$ with a very small overall volume change of 1.7%, which is one of the smallest volume changes for Na-ion cathodes and which is a crucial requisite for stable long-term cycling.

1. Introduction

The last two decades saw the establishment of Li-ion batteries as a leading technology for energy storage in portable and automotive applications.[1] In parallel, other storage technologies developed, trying to approach the performance of Li-ion and to surpass it in some aspect. Na-ion in particular is increasingly being studied, driven by the higher abundance of sodium and the potential for lower cost batteries.[2–4] These advantages can compensate the lower gravimetric energy density and make Na-ion a true contender for grid storage applications. Several review papers have been published recently, offering a complete overview of the numerous investigated electrode materials, both on the cathode and anode side of the battery.[5–10] The positive electrode is the main limiting factor for the gravimetric capacity of the battery[11] and no material has yet shown capacities equal to those of Li-ion battery cathodes (typically, stable specific energies of ≈750 Wh kg^{-1} for $LiCoO_2$,[12] ≈610 Wh kg^{-1} for $LiMn_2O_4$,[13] or ≈580 Wh kg^{-1} for $LiFePO_4$).[14] The three main classes of materials investigated as cathodes in Na-ion are: P2 or O3 transition metal oxides $NaTMO_2$,[15–18] where TM can be one or often several transition metals, and polyanionic compounds. The layered oxides have a large diversity of compositions due to the low tendency for TM migration into the slab space upon desodiation,[19] and multiple binary,[20] ternary,[21,22] and quaternary[23] mixtures of transition metals have been shown to work. The P2 structure, in particular, is promising and was shown to outperform O3 in terms of high mobility of sodium ions.[24] However, despite their rather high gravimetric energy density, often approaching or exceeding 600 Wh kg^{-1}, most layered materials tend to lose capacity upon cycling to high voltages.[9]

Polyanionic materials are structurally diverse compounds in which the arrangement of sodium, transition metals, and polyanions give rise to numerous structural frameworks.[25] At present, the most studied candidate materials have been vanadium-containing phosphates and fluorophosphates of compositions $Na_3V_2(PO_4)_3$[26–28] or $Na_3V_2(PO_4)_2F_3$.[29] This second compound, in particular, offers great promises. With an average operating potential of 3.9 V and a capacity of 128 mAh g^{-1}, its specific energy reaches 500 Wh kg^{-1}, an important milestone

Dr. M. Bianchini, Dr. P. Xiao, Prof. G. Ceder
Materials Science Division
LBNL
Berkeley, CA 94720, USA
E-mail: gceder@berkeley.edu
Dr. M. Bianchini, Prof. G. Ceder
Department of Materials Science and Engineering
UC Berkeley
Berkeley, CA 94720, USA
Dr. Y. Wang
Advanced Materials Lab
Samsung Research America
3 Van de Graaff Drive, Burlington, MA 01803, USA
Dr. Y. Wang
Department of Materials Science and Engineering
Massachusetts Institute of Technology
Cambridge, MA 02139, USA

DOI: 10.1002/aenm.201700514

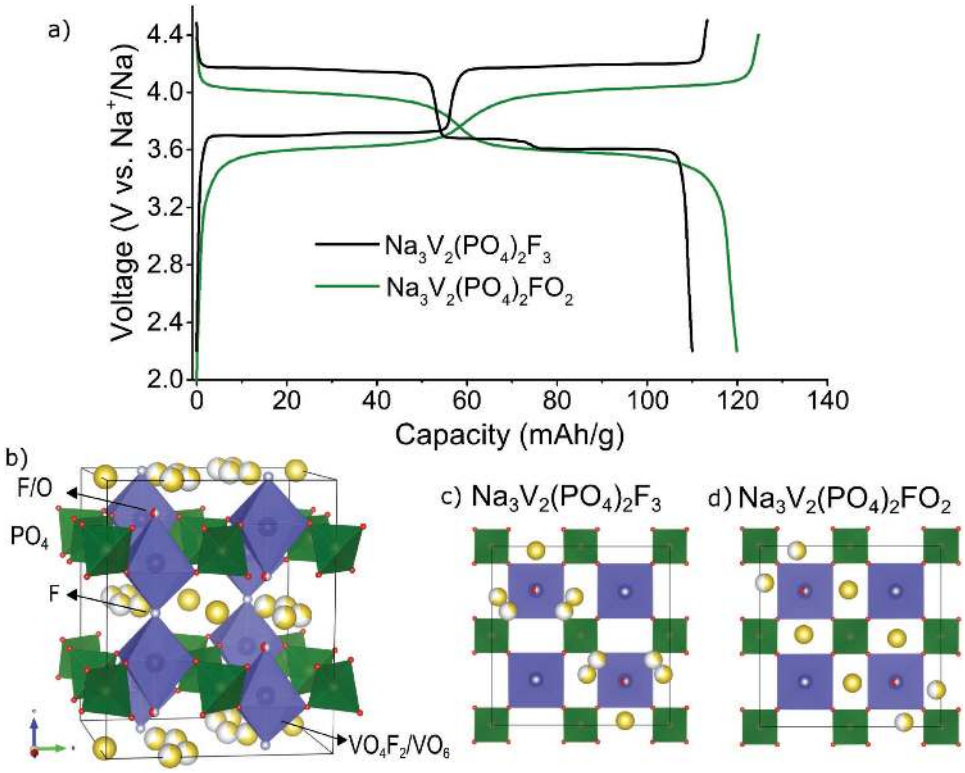

Figure 1. a) Electrochemical curve showing charge and discharge between 2.2 and 4.5 V for $Na_3V_2(PO_4)_2F_{3-2y}O_{2y}$ ($y = 0$ and $y = 1$), at C/10 rate. b) Crystal structure of $Na_3V_2(PO_4)_2F_{3-2y}O_{2y}$ (in orthorhombic space group Amam, applicable for $y \leq 0.2$. For $y > 0.2$, the structure belongs to the tetragonal $P4_2/mnm$ space group, where the only significant difference lies in the sodium distribution). c) Top view (*a*-*b* plane) of the crystal structure for $y = 0$, showing the sodium ordering observed in the orthorhombic structure. d) Top view (*a*-*b* plane) of the crystal structure for $y = 1$, showing the sodium ordering observed in the tetragonal structure.

that approaches the performance of commercial Li-ion battery cathodes.

$Na_3V_2(PO_4)_2F_3$ was first studied in 1999 by Le Meins et al.[30] who determined its crystal structure which is built on $V_2O_8F_3$ bioctahedra bridged by PO_4 tetrahedra. This framework creates pseudolayers in which sodium ions are inserted (**Figure 1**). The structure was initially solved in the tetragonal space group $P4_2/mnm$, but its symmetry has recently been revisited by Bianchini et al.,[31] who showed that the strong sodium interactions induce an orthorhombic distortion. Starting in 2006, Barker and co-workers[29,32] showed the promising capacity of this cathode when used versus lithium, sodium, and carbon anodes. Since then, several studies have shown that $Na_3V_2(PO_4)_2F_3$ can be synthesized by multiple routes, and when optimized can operate for thousands of cycles with negligible capacity fading.[33–41] $Na_3V_2(PO_4)_2F_3$ is actually the end member of a complete solid solution $Na_3V_2(PO_4)_2F_{3-2y}O_{2y}$,[36,42] where oxygen substitutes for fluorine in the vanadium-centered bioctahedra $V_2O_{8+2y}F_{3-2y}$ and creates vanadium of a higher average oxidation state ($V^{(3+y)+}$). Uncontrolled substitution due to unintended oxidation of the $Na_3V_2(PO_4)_2F_3$ compound has been the cause of discrepancies in the literature[43] because an increased oxygen content creates a slightly lower operating voltage (about 100 mV for the end member $y = 1$), a more sloping voltage curve caused by weaker sodium ordering (Na being screened by O^{2-} instead of F^-) and a smaller unit cell (because of the smaller ionic size of O^{2-} and the oxidation of V from 3+ to 4+). Two recent studies shed light on the full solid solution, clarifying the role of oxygen in modifying the crystal structure and electrochemical performance.[36,43] It was also shown that the orthorhombic distortion is only present for $y \leq 0.2$.

The scientific community concentrated primarily on $Na_3V_2(PO_4)_2F_3$ ($y = 0$), which can be easily synthesized by standard solid state techniques. This compound has a slightly higher energy density than $Na_3V_2(PO_4)_2FO_2$ (500 vs 495 Wh kg^{-1}). Moreover, an early report from Sauvage et al.[44] indicated $Na_3V_2(PO_4)_2FO_2$ to have poor capacity retention, as later confirmed by the study of Park et al.[36] However, the sample analyzed by Sauvage et al. was not phase pure, and Park et al. did not propose any explanation for their observed capacity fading in the $y = 0$ sample. It is worth mentioning though that, more recently, Serras et al.,[45] Xu et al.[46] and Zhao and co-workers[40,41] prepared $Na_3V_2(PO_4)_2FO_2$ by three distinct non-solid-state routes (hydro- and solvothermal) and reported excellent capacity retention for over 100 cycles[45,46] and up to 1000 cycles.[40] These findings show that the poor capacity retention previously observed is not intrinsic to the material, but may rather be due to side reactions originating from byproducts of the solid-state synthesis. Thus, there is no strong reason to a priori favor $Na_3V_2(PO_4)_2F_3$ over $Na_3V_2(PO_4)_2FO_2$.

As previously mentioned, the great promise of the (oxy)fluorophosphate family lies in the fact that ≈500 Wh kg^{-1} can be achieved through the (de)intercalation of two sodium ions, from $Na_3V_2(PO_4)_2F_{3-2y}O_{2y}$ to $NaV_2(PO_4)_2F_{3-2y}O_{2y}$.

However, a third Na^+ is still available at the end of charge where V is in oxidation state 4+ (at composition $NaV_2(PO_4)_2F_3$). The opportunity to further increase capacity by extracting this last Na has attracted significant efforts as the additional capacity would occur at a potential above 4.1 V, boosting the theoretical energy density beyond 800 Wh kg^{-1}. As a matter of fact, different groups[36,46–48] calculated that this deintercalation would happen at a potential too high to be reached within the stability window of the electrolyte, and as a result the third Na extraction has yet to be demonstrated. Zhang et al.[49] suggested that additional deintercalation is not the only route to improve the capacity of $Na_3V_2(PO_4)_2F_3$. In fact, three sodium cations in $Na_3V_2(PO_4)_2F_{3-2y}O_{2y}$ are distributed over four equivalent sites (Figure 1), creating an opportunity for inserting a 4th sodium accompanied by reduction of some V^{3+} to V^{2+}. They prepared $Na_4V_2(PO_4)_2F_3$ through mechanochemical synthesis, and subsequently electrochemically deintercalated it. This showed how extra sodium insertion is, in principle, a viable route to improve the energy density of $Na_3V_2(PO_4)_2F_3$. In practice, however, $Na_4V_2(PO_4)_2F_3$ cannot be obtained electrochemically from $Na_3V_2(PO_4)_2F_3$: operando X-Ray Diffraction (XRD)[49] showed that even discharge at low current to extremely low voltages (0.01 V, where electrolytes are not stable) only results in a biphasic composition of 40% $Na_3V_2(PO_4)_2F_3$–60% $Na_4V_2(PO_4)_2F_3$. Density Functional Theory (DFT) calculations, however, showed that the V^{3+}/V^{2+} redox couple should lie significantly higher for sodium insertion into $Na_3V_2(PO_4)_2F_3$.[48] Dacek et al.[48] rationalize the Na insertion problem by showing that the diffusivity of sodium drops by more than an order of magnitude at the exact composition $Na_3V_2(PO_4)_2F_3$, and a large energy barrier (811 meV) has to be overcome before additional sodium can be inserted. Once the insertion starts, however, diffusivity should increase again. They argue that it is not the migration barrier of sodium in the structure which is limiting, but rather the strong sodium-vacancy ordering which precludes the formation of mobile defects. As a consequence, the introduction of disorder in the vanadium or anion sublattice should lower the activation barrier for sodium insertion.

We confirm here experimentally that the strong ordering and electrostatic repulsion between Na^+ ions is responsible for the difficulty in achieving the low-voltage insertion plateau in $Na_3V_2(PO_4)_2F_3$, and that insertion can be enabled by introducing disorder in the cation lattice through aluminum substitution. Moreover we show how the oxygen-substituted $Na_3V_2(PO_4)_2FO_2$ enables sodium insertion at ≈1.6 V, close to the theoretically predicted voltage. We finally investigate this insertion in detail through operando X-ray diffraction.

2. Results and Discussion

2.1. Sodium Insertion into $Na_3V_2(PO_4)_2FO_2$

Figure 2 shows the electrochemical charge and discharge curves of $Na_3V_2(PO_4)_2F_{3-2y}O_{2y}$ for $y = 0$ and $y = 1$. Consistently with the report of Zhang et al.,[49] a very small amount of additional capacity is obtained for the $y = 0$ sample when discharged to 1 V. On the other hand, we observe for the first time how $Na_3V_2(PO_4)_2FO_2$ can uptake a fourth sodium well above 1.3 V. This intercalation is observed in Figure 2 as a plateau at 1.57 V, and as a peak in the dQ/dV curve (inset). According to the Gibbs phase rule, a flat electrochemical curve like the one observed here suggests a two-phase reaction mechanism. Such step allows for the intercalation of an entire extra sodium, for an additional capacity of 65 mAh g^{-1}. Considering this, the theoretical energy density of $Na_3V_2(PO_4)_2FO_2$ when cycled in the range $Na_4V_2(PO_4)_2FO_2$–$NaV_2(PO_4)_2FO_2$ is about 600 Wh kg^{-1}, the highest among polyanionic compositions for sodium ion batteries. However, one should note the large voltage difference between the two plateaus at 3.6 and 4 V, and this new plateau at 1.6 V. While our work proves that this extra capacity is accessible in the fluorophosphate material, the voltage of this insertion plateau will need to be increased to make it practically relevant. The origin of the possibility to insert the 4th sodium lies in the strong screening effect of O^{2-} anions, which are placed on the axis normal to the square connecting the 4 Na^+ (Figure 2c) and weakens the electrostatic repulsion between the Na^+ ions. In $Na_3V_2(PO_4)_2F_3$ the presence of F^- in this position creates a less effective screening.

More quantitative considerations can be obtained by DFT calculations (**Figure 3**). The voltage in the well-known sodiation regime $1 \le x \le 3$ is in good agreement with previous theoretical calculations,[36] although the values are slightly underestimated compared to the experimental ones. The V^{3+}/V^{4+} redox couple in $Na_3V_2(PO_4)_2F_3$ occurs at higher voltage than the V^{4+}/V^{5+} in $Na_3V_2(PO_4)_2FO_2$, due to the stronger inductive effect of the more electronegative F^- anions compared to O^{2-}.[25,50] Regarding the $3 \le x \le 4$ regime, we find that the average potential for sodium insertion into $Na_3V_2(PO_4)_2FO_2$ is 2.1 V; at the same time the potential calculated to insert a small amount of sodium (e.g., to reach $Na_{3.125}V_2(PO_4)_2FO_2$) is 1.9 V, closer to the experimental value. These analogous values for $Na_3V_2(PO_4)_2F_3$ are 1.85 and 1.67 V, respectively. The relative equilibrium potentials calculated for the Na insertion into $Na_3V_2(PO_4)_2FO_2$ and $Na_3V_2(PO_4)_2F_3$ confirm that insertion into the former is energetically more favorable than in the latter, due to the decreased electrostatic repulsion between Na^+ cations (a reduction that can be estimated to about 200–300 meV). The fact that the potential for inserting a small amount of Na is lower than that for full insertion from $Na_3V_2(PO_4)_2F_{3-2y}O_{2y}$ to $Na_4V_2(PO_4)_2F_{3-2y}O_{2y}$ reflects the fact that the equilibrium thermodynamics implies two-phase behavior. However, nucleation of a second phase is often difficult at room temperature and a metastable incremental insertion (solid solution) can be the mechanism by which a single particle crosses the phase transformation.[51] This metastable transformation mechanism still leads to particles being in either the $Na_3V_2(PO_4)_2FO_2$ or $Na_4V_2(PO_4)_2FO_2$ state,[52] consistent with the two-phase behavior seen in operando XRD (**Figure 4**). The calculated equilibrium voltages for the 4th Na insertion are about 0.5 V higher than experimental values, supporting the fact that sodium insertion is not thermodynamically hindered, but mostly precluded by the overpotential required to disrupt the stable Na-vacancy ordering at the pristine composition.

To further detail the sodium insertion into $Na_3V_2(PO_4)_2FO_2$, we conducted operando X-ray diffraction during a full electrochemical cycle. Figure 4 shows a contour plot of the evolution of the (115) Bragg peak upon sodium extraction (to $NaV_2(PO_4)_2FO_2$), reinsertion (to $Na_4V_2(PO_4)_2FO_2$), and final

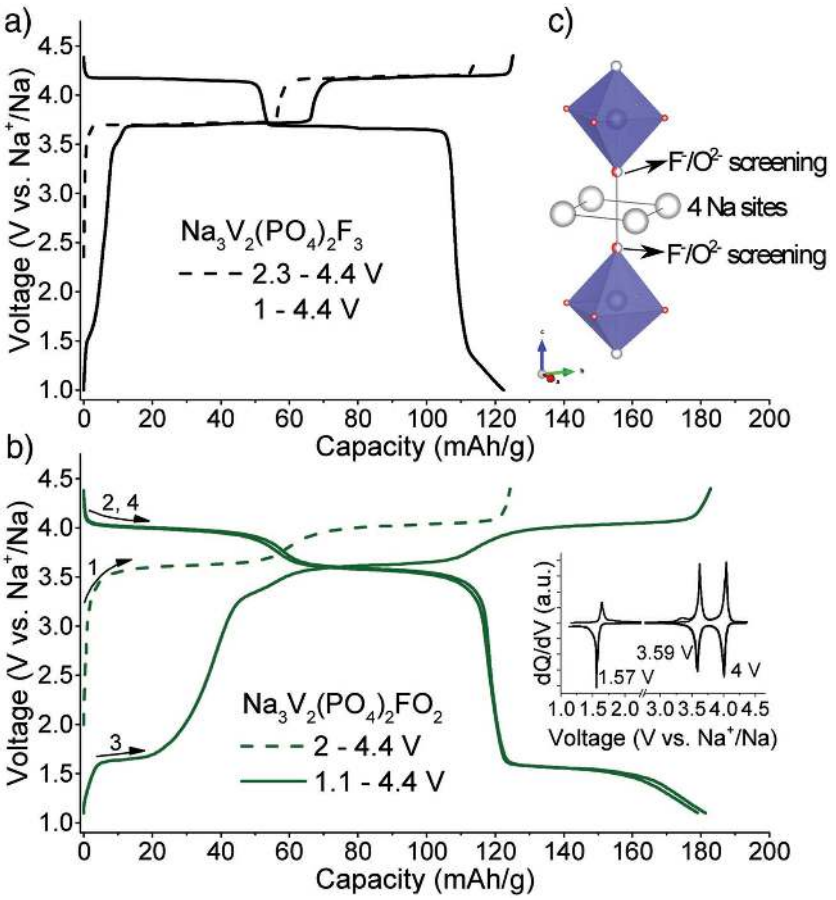

Figure 2. a) The electrochemical charge and discharge curve of $Na_3V_2(PO_4)_2F_3$ cycled between 1 and 4.4 V at C/20. Note that there is little capacity below 2 V. b) Electrochemical charge and discharge curve of $Na_3V_2(PO_4)_2FO_2$ (same rate and voltage cut-off). Additional capacity below 2 V is observed as sodium is inserted to reach composition $Na_4V_2(PO_4)_2FO_2$, through a plateau at 1.57 V. c) Structure fragment showing the four equivalent sodium sites in $Na_3V_2(PO_4)_2F_{3-2y}O_{2y}$ and the position of the F/O anions screening the repulsive Coulombic interaction among them.

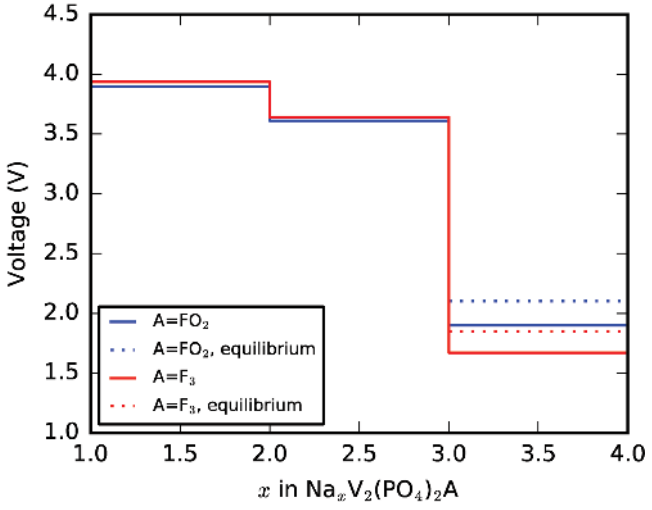

Figure 3. The computed voltage curves of $Na_xV_2(PO_4)_2F_{3-2y}O_{2y}$ in the range $1 \le x \le 4$, for $y = 0$ (red) and $y = 1$ (blue). The dotted curves refer to the average equilibrium potential calculated between compositions $Na_{3-4}V_2(PO_4)_2F_{3-2y}O_{2y}$, while the full lines are calculated in the region $Na_{3-3.125}V_2(PO_4)_2F_{3-2y}O_{2y}$.

extraction to regain the initial $Na_3V_2(PO_4)_2FO_2$, proving the reversibility of the intercalation reaction. The regime $Na_{3-1}V_2(PO_4)_2FO_2$ has already been studied in detail by a synchrotron operando study of Sharma et al.[53] Our experiment confirms the reactions and unit cell parameters observed in that work. They describe a sequence of biphasic reactions upon charge and discharge, with intermediate Na-ordered phases typical of this class of compounds. In our experiment, despite the more limited resolution of an in-house diffractometer, we can distinguish at least two biphasic reactions upon both charge and discharge, separated by the intermediate composition $Na_2V_2(PO_4)_2FO_2$ (biphasic reactions are characterized by peaks losing intensity and new peaks concurrently gaining intensity at a different 2θ position, as opposed to the continuous peak shift one would observe for a solid solution reaction mechanism). We can then use profile-matching refinement (LeBail fit) to determine the cell parameters of significant compositions: for the desodiated end-member $NaV_2(PO_4)_2FO_2$, we find in the $P4_2/mnm$ space group, $a = b = 8.904(3)$ Å, $c = 10.805(3)$ Å, $V = 856.7(4)$ Å^3, in good agreement with the values reported by Sharma et al.[53] This gives a relative volume contraction upon charge of

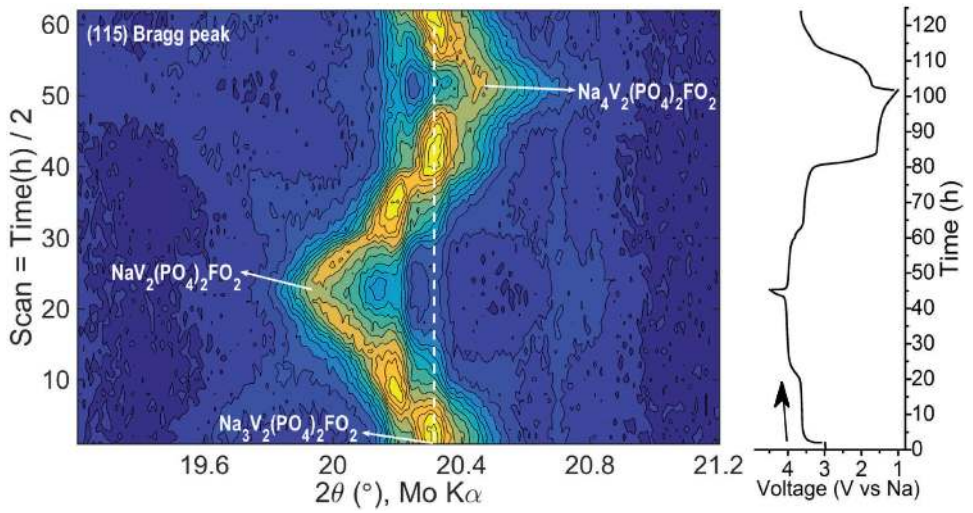

Figure 4. Contour plot showing the evolution of the (115) Bragg peak during operando XRD. $Na_3V_2(PO_4)_2FO_2$ was first charged at C/40 to 4.5 V, then discharged to 1 V, and finally charged back to the initial state at 3.6 V. Diffraction scans were continuously collected for a scan duration of 2 h. The dashed vertical line indicates the position of the Bragg peak at pristine composition $Na_3V_2(PO_4)_2FO_2$.

$\Delta V/V = -0.7\%$ with respect to the pristine compound (**Table 1**). We note that the cell parameters variation is anisotropic: a and b shrink upon sodium extraction, while c increases, resulting in a small overall volume variation. Upon Na insertion, we observe for the first time the end-member $Na_4V_2(PO_4)_2FO_2$, which appears through a biphasic reaction, consistent with the flat electrochemical curve. The unit cell parameters we retrieve from the operando data are: $a = b = 9.092(3)$ Å, $c = 10.549(3)$ Å, $V = 872.0(4)$ Å^3. This shows a very low unit cell expansion of only $\Delta V/V = +1\%$ upon insertion of the 4th sodium. Notably, this means an overall volume variation during the exchange of three sodium ions of $|\Delta V|/V = 1.7\%$, possibly the smallest ever reported for a sodium-ion battery electrode. One should note that this value is significantly smaller than the one potentially obtainable for $Na_3V_2(PO_4)_2F_3$, which upon charge contracts by −3%, and during discharge to $Na_4V_2(PO_4)_2F_3$ expands further by +3.2%, for a total variation $|\Delta V|/V = 6.2\%$. These findings support once more the great potential of $Na_{1-4}V_2(PO_4)_2FO_2$ as Na-ion positive electrode.

Table 1. Unit cell parameters of the synthesized $Na_3V_{2-z}Al_z(PO_4)_2F_3$ (z = 0, 0.1, 0.2, 0.3) and $Na_xV_2(PO_4)_2FO_2$ (x = 3, 1, 4). Parameters are obtained from LeBail fit of X-ray diffraction data, using the Amam space group for all $Na_3V_{2-z}Al_z(PO_4)_2F_3$, and $P4_2/mnm$ for $Na_3V_2(PO_4)_2FO_2$. Data obtained from operando experiment marked with*.

Material	a [Å]	b [Å]	c [Å]	Vol [Å^3]
$Na_3V_2(PO_4)_2F_3$	9.025(1)	9.043(1)	10.746(1)	877.0(1)
$Na_3V_{1.9}Al_{0.1}(PO_4)_2F_3$	9.016(1)	9.032(1)	10.732(1)	874.0(1)
$Na_3V_{1.8}Al_{0.2}(PO_4)_2F_3$	9.002(3)	9.026(3)	10.716(3)	870.9(3)
$Na_3V_{1.7}Al_{0.3}(PO_4)_2F_3$	8.990(1)	9.010(1)	10.704(1)	867.1(2)
$Na_3V_2(PO_4)_2FO_2$	9.012(1)	9.012(1)	10.627(2)	863.1(2)
$NaV_2(PO_4)_2FO_2$*	8.904(3)	8.904(3)	10.805(3)	856.7(4)
$Na_4V_2(PO_4)_2FO_2$*	9.092(3)	9.092(3)	10.549(3)	872.0(4)

2.2. Sodium Extraction and Insertion from/into $Na_3V_{2-z}Al_z(PO_4)_2F_3$

The fact that sodium insertion was obtained for the $y = 1$ composition raises the question whether the $y = 0$ compound can also be modified to allow sodium intercalation. It was recently shown that the shape of the electrochemical curve of $Na_3V_2(PO_4)_2F_3$ is due to the fact that sodium, being weakly screened by F^-, can order in complex patterns while it is extracted.[39] Every time an ordering of Na occurs, some overpotential is required to disrupt it. Dacek et al.[48] calculate activation energies for sodium diffusion as high as 811 meV for $Na_3V_2(PO_4)_2F_3$, 556 meV for $Na_2V_2(PO_4)_2F_3$ and 353 meV for $NaV_2(PO_4)_2F_3$, while for intermediate compositions between these end-members activation energies are in the range 100–300 meV.[48] In the following, we use aluminum substitution of vanadium into $Na_3V_2(PO_4)_2F_3$ to disrupt sodium ordering and examine the electrochemical properties of the $Na_3V_{2-z}Al_z(PO_4)_2F_3$ compounds, upon both sodium insertion and extraction.

For small amounts of aluminum ($z \leq 0.3$), pure compositions could be obtained. The Al substitution was confirmed by the steady decrease in unit cell parameters for increasing z (Table 1; Figure S3, Supporting Information). Consistent with the smaller ionic radius of Al^{3+} as compared to V^{3+} (0.54 vs 0.64 Å), the unit cell decreased from 877 Å^3 ($z = 0$) to 867 Å^3 ($z = 0.3$). The strategy of aluminum substitution has also, in principle, the beneficial effect of increasing the gravimetric capacity of the material, provided that the substitution does not diminish the available redox-active ions. This idea was implemented for example by Lalère et al.[28] for $Na_3V_2(PO_4)_3$, in which the accessibility of the V^{4+}/V^{5+} redox couple provides an excess of oxidation capacity. It is not clear, a priori, if this would be viable in $Na_3V_2(PO_4)_2F_3$. Matts et al.[47] concluded that the V^{4+}/V^{5+} redox couple can be active in $Na_3V_2(PO_4)_2F_3$, so in principle substitution of V by Al should not decrease the capacity in the high-voltage region, while allowing for additional sodium insertion.

However the sample considered in that study had considerable NASICON impurities and the electrochemical curve reported for their gallium-doped sample only showed ≈65 mAh g^{-1} of capacity above 2 V, which is the capacity that would be obtained if the V^{4+}/V^{5+} redox couple was not active. Hence, accessibility of V^{4+}/V^{5+} in the fluorophosphate remains an open question.

Figure 5 shows $Na_3V_{2-z}Al_z(PO_4)_2F_3$ when cycled between 1 and 4.4 V. The electrochemical curves are smoother than the one of pure $Na_3V_2(PO_4)_2F_3$ (Figure 1), similar to what is obtained by substituting O for F in $Na_3V_2(PO_4)_2F_{3-2y}O_{2y}$. Al substitution clearly enables insertion of more Na at low voltage (Figure 5b). The insertion occurs at 1.3 V, lower than in $Na_3V_2(PO_4)_2FO_2$ and below what is considered a safe voltage against electrolyte reduction (above 1.4–1.5 V). The sodium insertion is confirmed by in situ X-ray diffraction (Figure S4, Supporting Information). The electrochemical curve in the regime $Na_{3-4}V_{2-z}Al_z(PO_4)_2F_3$ is significantly less flat than in $Na_{3-4}V_{2-z}Al_z(PO_4)_2FO_2$; since the in situ XRD data support in both cases a biphasic reaction mechanism, such a sloping discharge curve likely indicates a poorer kinetics of Na^+ ions for the former compounds.

In order to demonstrate that Al substitution improves the kinetics near $x = 3$, where Na ordering has been shown to lead to high sodium mobility barriers, we conducted a slow GITT measurement (Galvanostatic Intermittent Titration Technique). **Figure 6** compares the potential relaxation and overpotential between $3 \le x \le 3.2$ for the $z = 0$ and $z = 0.3$ samples. One notes that the overpotential required for discharge is significantly reduced in $Na_3V_{1.7}Al_{0.3}(PO_4)_2F_3$ compared to $Na_3V_2(PO_4)_2F_3$. This is exactly the composition at which the Na ordering occurs.

As the aluminum amount increases in $Na_3V_{2-z}Al_z(PO_4)_2F_3$, the gravimetric capacity is reduced (Figure 5a). Moreover, the capacity is lost on the highest voltage plateau (at 4.1 V), while the lower one (at 3.6 V) retains a constant capacity, confirming that the Al substitution reduces the amount of V^{3+}/V^{4+} redox couple available, and no extra V^{4+}/V^{5+} can be accessed to compensate. In this scenario, the composition reached at the end of charge would be $Na_{1+z}V_{2-z}Al_z(PO_4)_2F_3$, in rather good agreement with our electrochemical measurements (inset in Figure 5a). This finding finally supports the speculation that the V^{4+}/V^{5+} redox couple is not active in $Na_3V_2(PO_4)_2F_3$ (at least not below 4.7 V). The fact that the V^{4+}/V^{5+} couple can be accessed in $Na_3V_2(PO_4)_2FO_2$ but not in $Na_3V_2(PO_4)_2F_3$ can be rationalized as follows: $Na_3V_2(PO_4)_2F_3$ is

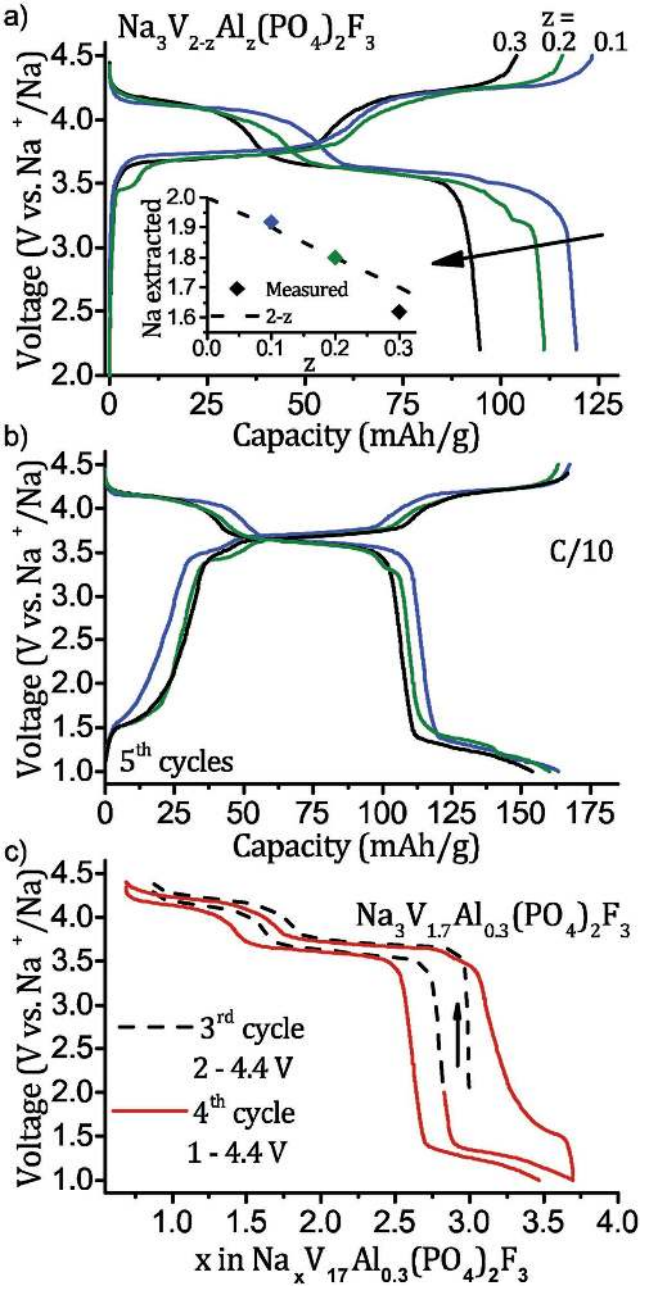

Figure 5. a) Electrochemical charge and discharge curves of $Na_3V_{2-z}Al_z(PO_4)_2F_3$ ($z = 0.1$, 0.2, 0.3) cycled at C/10 rate between 2.2 and 4.5 V, showing that the obtained capacity decreases with increasing z. The inset shows the amount of sodium extracted upon charge. b) Additional sodium insertion when $Na_3V_{2-z}Al_z(PO_4)_2F_3$ is discharged to 1 V. c) $Na_3V_{1.7}Al_{0.3}(PO_4)_2F_3$ cycled between 1 and 4.4 V, as a function of sodium content.

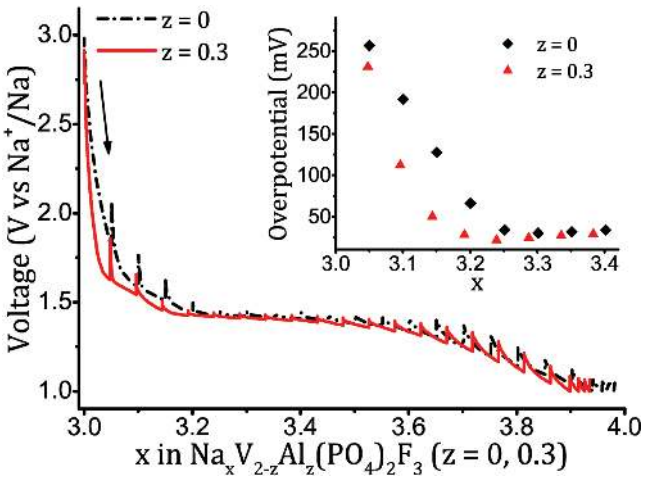

Figure 6. GITT electrochemical discharge curves of $Na_3V_{2-z}Al_z(PO_4)_2F_3$ ($z = 0$ (black dashed) and $z = 0.3$ (red)). The same GITT conditions are employed, as reported in the Experimental Section. Inset: overpotential between discharge and relax intervals, showing lower values for the Al-substituted sample, with a more pronounced difference in $3 \le x \le 3.2$.

built by bioctahedra with F—V—F—V—F bonds of rather regular length (1.97–1.98 Å), in agreement with many reported V^{3+} octahedral environments.[54,55] $Na_3V_2(PO_4)_2FO_2$, on the other hand, has irregular bond lengths,[36,56,57] consistent with the fact that V^{4+} often forms a single shorter vanadyl bond (in a bioctahedra of $Na_3V_2(PO_4)_2FO_2$, there is an axial bond sequence O—V—F—V—O with bond lengths 1.6–2.1–2.1–1.6 Å). This trend showing less regular bond lengths as vanadium is oxidized agrees well with the comprehensive review by Schindler et al.[55] on the crystal chemistry of vanadium; the review also shows that further oxidation from V^{4+} to V^{5+} often causes the difference between long and short bond to be even more pronounced (from average 1.60–2.26 in V^{4+} to 1.58–2.32 on V^{5+}). Other intercalation systems have the same bond-length trend upon oxidation, whether they contain V—O—V—O chains, as in $LiVPO_4O$,[58] or V—F—V—F chains, as in $LiVPO_4F$.[59] One can then understand how the structure of $Na_3V_2(PO_4)_2FO_2$, built on asymmetric O—V—F—V—O bonds, can more easily accommodate V^{4+} and V^{5+} cations. However, $Na_3V_2(PO_4)_2F_3$ has symmetric F—V—F—V—F bonds, thus favoring a regular V^{3+} environment. Upon oxidation, it needs to distort these bonds into an energetically unfavorable arrangement. The very recent observation by Bianchini et al.[39] using operando synchrotron XRD that, at composition $NaV^{IV}{}_2(PO_4)_2F_3$, V^{4+} can even undergo disproportionation seems consistent with the lack of stability of V^{4+} in a very symmetric environment (this was very recently confirmed by X-Ray Absorption Near Edge Structure (XANES) and Nuclear Magnetic Resonance (NMR) by Broux et al.).[60] The end-member would then be more accurately written as $NaV^{III}V^{V}(PO_4)_2F_3$, where within the bioctahedron, one octahedron is distorted and one is not. These considerations show how extraction of Na beyond $NaV_2(PO_4)_2F_3$ (and average oxidation beyond V^{4+}) is very unlikely, explaining why DFT predicts it to happen only at voltages well above 4.5 V. Considering that the most oxidized state for vanadium is 5+, sodium extraction is also not possible beyond $NaV_2(PO_4)_2FO_2$, leaving sodium insertion as the most accessible way to improve the performance of this family of fluorophosphates.

3. Conclusion

In conclusion, we have shown for the first time how sodium insertion into $Na_3V_2(PO_4)_2FO_2$ at 1.57 V can extend its gravimetric energy density to 600 Wh kg^{-1} reaching the end member $Na_4V_2(PO_4)_2FO_2$. We demonstrated that this extended cycling range, albeit extending over a large voltage range, comes with extremely small volume change, a promising aspect for good capacity retention. Thus $Na_3V_2(PO_4)_2FO_2$ should not a priori be neglected in favor of $Na_3V_2(PO_4)_2F_3$ as a positive electrode material of choice for Na-ion batteries. Especially when observing that recent literature[40,45,46] has shown $Na_3V_2(PO_4)_2FO_2$ to be immune to capacity fading, contradicting the previous belief. We have also experimentally demonstrated that Al substitution into $Na_3V_2(PO_4)_2F_3$ decreases the energy barrier hindering sodium insertion toward $Na_4V_2(PO_4)_2F_3$. However, this insertion comes at too low a potential (1.3 V) to be practically viable. We suggest that doping with other redox-active cations may produce the synergistic effect of disrupting Na orderings in the structure, while at the same time providing extra redox capacity for sodium insertion at higher voltage.

4. Experimental Section

$Na_3V_2(PO_4)_2F_3$ (Figure S1, Supporting Information) was synthesized by standard solid state reaction between stoichiometric amounts of VPO_4 and NaF, as previously reported.[29] For the aluminum-doped samples, stoichiometric amounts of VPO_4 were replaced by $AlPO_4$ (Sigma). $Na_3V_2(PO_4)_2FO_2$ was also synthesized by solid state route (Figure S2, Supporting Information), according to Park et al.[36] by reacting stoichiometric amounts of VPO_4, $VOPO_4$, NaF, and Na_2CO_3. VPO_4 and $VOPO_4$ required for the reactions discussed above were prepared as described by Broux et al.[43] VPO_4 is made by reduction of a stoichiometric mixture of V_2O_5 and $NH_4H_2PO_4$ under hydrogen(2%)/argon atmosphere at 800 C. $VOPO_4$ is subsequently made by oxidation of VPO_4 fired in air at 700 C. X-ray diffraction was conducted on a Rigaku diffractometer, in Bragg–Brentano geometry using Cu Kα radiation. In situ/operando experiments were conducted in the custom made electrochemical cell, in Bragg–Brentano geometry but using Mo Kα radiation in a Bruker diffractometer. Every scan was collected for 2 h, while the battery was cycled at C/40 rate (calculated so that 40 h were required for the first charge). Electrodes for electrochemical characterization were prepared by mixing the active materials with carbon black and ball milling them for 30 min in a Fritsh Pulverisette, followed by addition of PTFE as binder, such that the overall electrode composition was 80% AM – 16% Carbon – 4% PTFE. Standard 2032 coin cells were assembled in an argon-filled glovebox, using 1 M $NaPF_6$ in EC:DEC (1:1 ethylene carbonate-dimethyl carbonate) as electrolyte and sodium metal as counter electrode. Positive electrode loadings were typically 10 mg cm^{-2}. Electrochemical tests were conducted on an Arbin instrument. GITT electrochemical tests were conducted in the same configuration as above, with discharge at C/50 rate (calculated as above) and discharge/relax times alternated every 75 min. Calculations were performed using density functional theory, as implemented in the Vienna ab initio simulation package,[61–63] by using the projector-augmented wave method.[63,64] A kinetic energy cutoff of 520 eV was chosen for the plane-wave basis set, and Γ-centered k-point mesh was used with a reciprocal space discretization of 0.25 $Å^{-1}$. The GGA (Generalized Gradient Approximation) - PBE (Perdew-Burke-Ernzerhof) exchange correlation functional[65] with the rotationally invariant scheme of Hubbard-U correction[66] was applied to calculate the voltages, and a value of U_{eff} = 4 eV was employed, consistent with previous theoretical studies of vanadium fluorophosphates.[36,46] Na orderings within the $Na_xV_2(PO_4)_2F_{3-2y}O_{2y}$ framework were found with the basin-hopping algorithm as described in ref. [46].

Supporting Information

Supporting Information is available from the Wiley Online Library or from the author.

Acknowledgements

This work was supported by Samsung Advanced Institute of Technology. The authors acknowledge Dong-Hwa Seo and Steve Dacek for fruitful discussion. Computational resources from the National Energy Research Scientific Computing Center (NERSC) and from the Extreme Science and Engineering Discovery Environment (XSEDE) are gratefully acknowledged.

Conflict of Interest

The authors declare no conflict of interest.

Keywords

batteries, electrodes, Na-ions, operando, structure–property relationships

Received: February 24, 2017
Revised: March 28, 2017
Published online: May 16, 2017

[1] R. Van Noorden, *Nature* **2014**, *507*, 26.
[2] B. L. Ellis, L. F. Nazar, *Curr. Opin. Solid State Mater. Sci.* **2012**, *16*, 168.
[3] J.-M. Tarascon, *Nat. Chem.* **2010**, *2*, 510.
[4] H. Pan, Y.-S. Hu, L. Chen, *Energy Environ. Sci.* **2013**, *6*, 2338.
[5] S.-W. Kim, D.-H. Seo, X. Ma, G. Ceder, K. Kang, *Adv. Energy Mater.* **2012**, *2*, 710.
[6] M. D. Slater, D. Kim, E. Lee, C. S. Johnson, *Adv. Funct. Mater.* **2013**, *23*, 947.
[7] N. Yabuuchi, K. Kubota, M. Dahbi, S. Komaba, *Chem. Rev.* **2014**, *114*, 1163611682.
[8] E. Irisarri, A. Ponrouch, M. R. Palacin, *J. Electrochem. Soc.* **2015**, *162*, A2476.
[9] K. Kubota, S. Komaba, *J. Electrochem. Soc.* **2015**, *162*, A2538.
[10] D. Kundu, E. Talaie, V. Duffort, L. F. Nazar, *Angew. Chem., Int. Ed.* **2015**, *54*, 3431.
[11] X. Xiang, K. Zhang, J. Chen, *Adv. Mater.* **2015**, *27*, 5343.
[12] K. Mizushima, P. C. Jones, P. J. Wiseman, J. B. Goodenough, *Mater. Res. Bull.* **1980**, *15*, 783.
[13] M. M. Thackeray, P. J. Johnson, L. A. de Picciotto, P. G. Bruce, J. B. Goodenough, *Mater. Res. Bull.* **1984**, *19*, 179.
[14] A. K. Padhi, K. S. Nanjundaswamy, J. B. Goodenough, *J. Electrochem. Soc.* **1997**, *144*, 1188.
[15] J. J. Braconnier, C. Delmas, C. Fouassier, P. Hagenmuller, *Mater. Res. Bull.* **1980**, *15*, 1797.
[16] R. Berthelot, D. Carlier, C. Delmas, *Nat. Mater.* **2011**, *10*, 74.
[17] J. Billaud, R. J. Clement, A. R. Armstrong, J. Canales-Vazquez, P. Rozier, C. P. Grey, P. G. Bruce, *J. Am. Chem. Soc.* **2014**, *136*, 17243.
[18] R. J. Clement, P. G. Bruce, C. P. Grey, *J. Electrochem. Soc.* **2015**, *162*, A2589.
[19] S. P. Ong, V. L. Chevrier, G. Hautier, A. Jain, C. Moore, S. Kim, X. Ma, G. Ceder, *Energy Environ. Sci.* **2011**, *4*, 3680.
[20] N. Yabuuchi, M. Kajiyama, J. Iwatate, H. Nishikawa, S. Hitomi, R. Okuyama, R. Usui, Y. Yamada, S. Komaba, *Nat. Mater.* **2012**, *11*, 512.
[21] I. Hasa, D. Buchholz, S. Passerini, B. Scrosati, J. Hassoun, *Adv. Energy Mater.* **2014**, *4*, 1400083.
[22] L. Liu, X. Li, S.-H. Bo, Y. Wang, H. Chen, N. Twu, D. Wu, G. Ceder, *Adv. Energy Mater.* **2015**, *5*, 1500944.
[23] X. Li, Y. Wang, D. Wu, L. Liu, S.-H. Bo, G. Ceder, *Chem. Mater.* **2016**, *28*, 6575.
[24] Y. Mo, S. P. Ong, G. Ceder, *Chem. Mater.* **2014**, *26*, 5208.
[25] C. Masquelier, L. Croguennec, *Chem. Rev.* **2013**, *113*, 6552.
[26] Y. Uebou, T. Kiyabu, S. Okada, J.-I. Yamaki, *Rep. Inst. Adv. Mater. Study, Kyushu Univ.* **2002**, *16*, 1.
[27] Z. Jian, W. Han, X. Lu, H. Yang, Y.-S. Hu, J. Zhou, Z. Zhou, J. Li, W. Chen, D. Chen, L. Chen, *Adv. Energy Mater.* **2013**, *3*, 156.
[28] F. Lalere, V. Seznec, M. Courty, R. David, J. N. Chotard, C. Masquelier, *J. Mater. Chem. A* **2015**, *3*, 16198.
[29] R. K. B. Gover, A. Bryan, P. Burns, J. Barker, *Solid State Ionics* **2006**, *177*, 1495.
[30] J. M. Le Meins, M. P. Crosnier-Lopez, A. Hemon-Ribaud, G. Courbion, *J. Solid State Chem.* **1999**, *148*, 260.
[31] M. Bianchini, N. Brisset, F. Fauth, F. Weill, E. Elkaim, E. Suard, C. Masquelier, L. Croguennec, *Chem. Mater.* **2014**, *26*, 4238.
[32] J. Barker, R. K. Gover, P. Burns, A. J. Bryan, *Electrochem. Solid-State Lett.* **2006**, *9*, A190.
[33] R. Shakoor, D.-H. Seo, H. Kim, Y.-U. Park, J. Kim, S.-W. Kim, H. Gwon, S. Lee, K. Kang, *J. Mater. Chem.* **2012**, *22*, 20535.
[34] A. Ponrouch, R. Dedryvere, D. Monti, A. E. Demet, J. M. Ateba Mba, L. Croguennec, C. Masquelier, P. Johansson, M. R. Palacin, *Energy Environ. Sci.* **2013**, *6*, 2361.
[35] K. Chihara, A. Kitajou, I. D. Gocheva, S. Okada, J.-I. Yamaki, *J. Power Sources* **2013**, *227*, 80.
[36] Y.-U. Park, D.-H. Seo, H. Kim, J. Kim, S. Lee, B. Kim, K. Kang, *Adv. Funct. Mater.* **2014**, *24*, 4603.
[37] W. Song, X. Cao, Z. Wu, J. Chen, Y. Zhu, H. Hou, Q. Lan, X. Ji, *Langmuir* **2014**, *30*, 12438.
[38] Z. Liu, Y.-Y. Hu, M. T. Dunstan, H. Huo, X. Hao, H. Zou, G. Zhong, Y. Yang, C. P. Grey, *Chem. Mater.* **2014**, *26*, 2513.
[39] M. Bianchini, F. Fauth, N. Brisset, F. Weill, E. Suard, C. Masquelier, L. Croguennec, *Chem. Mater.* **2015**, *27*, 3009.
[40] Y. Qi, L. Mu, J. Zhao, Y.-S. Hu, H. Liu, S. Dai, *Angew. Chem.* **2015**, *127*, 10049.
[41] J. Zhao, L. Mu, Y. Qi, Y.-S. Hu, H. Liu, S. Dai, *Chem. Commun.* **2015**, *51*, 7160.
[42] P. Serras, V. Palomares, A. Goni, I. G. de Muro, P. Kubiak, L. Lezama, T. Rojo, *J. Mater. Chem.* **2012**, *22*, 22301.
[43] T. Broux, T. Bamine, F. Fauth, L. Simonelli, W. Olszewski, C. Marini, M. Menetrier, D. Carlier, C. Masquelier, L. Croguennec, *Chem. Mater.* **2016**, *28*, 7683.
[44] F. Sauvage, E. Quarez, J. M. Tarascon, E. Baudrin, *Solid State Sci.* **2006**, *8*, 1215.
[45] P. Serras, V. Palomares, P. Kubiak, L. Lezama, T. Rojo, *Electrochem. Commun.* **2013**, *34*, 344.
[46] M. Xu, P. Xiao, S. Stauffer, J. Song, G. Henkelman, J. B. Goodenough, *Chem. Mater.* **2014**, *26*, 3089.
[47] I. L. Matts, S. Dacek, T. K. Pietrzak, R. Malik, G. Ceder, *Chem. Mater.* **2015**, *27*, 6008.
[48] S. T. Dacek, W. D. Richards, D. A. Kitchaev, G. Ceder, *Chem. Mater.* **2016**, *28*, 5450.
[49] B. Zhang, R. Dugas, G. Rousse, P. Rozier, A. M. Abakumov, J.-M. Tarascon, *Nat. Commun.* **2016**, *7*, 10308.
[50] A. Manthiram, J. B. Goodenough, *J. Solid State Chem.* **1987**, *71*, 349.
[51] R. Malik, F. Zhou, G. Ceder, *Nat. Mater.* **2011**, *10*, 587.
[52] R. Malik, A. Abdellahi, G. Ceder, *J. Electrochem. Soc.* **2013**, *160*, A3179.
[53] N. Sharma, P. Serras, V. Palomares, H. E. A. Brand, J. Alonso, P. Kubiak, M. L. Fdez-Gubieda, T. Rojo, *Chem. Mater.* **2014**, *26*, 3391.
[54] P. Y. Zavalij, M. S. Whittingham, *Acta Crystallogr., Sect. B: Struct. Sci.* **1999**, *55*, 627.
[55] M. Schindler, F. C. Hawthorne, W. H. Baur, *Chem. Mater.* **2000**, *12*, 1248.
[56] W. Massa, O. V. Yakubovich, O. V. Dimitrova, *Solid State Sci.* **2002**, *4*, 495.
[57] A. A. Tsirlin, R. Nath, A. M. Abakumov, Y. Furukawa, D. C. Johnston, M. Hemmida, H. A. Krug von Nidda, A. Loidl, C. Geibel, H. Rosner, *Phys. Rev. B* **2011**, *84*, 014429.

[58] M. Bianchini, J. M. Ateba-Mba, P. Dagault, E. Bogdan, D. Carlier, E. Suard, C. Masquelier, L. Croguennec, *J. Mater. Chem. A* **2014**, *2*, 10182.
[59] B. L. Ellis, T. Ramesh, L. J. Davis, G. R. Goward, L. F. Nazar, *Chem. Mater.* **2011**, *23*, 5138.
[60] T. Broux, T. Bamine, L. Simonelli, L. Stievano, F. Fauth, M. Menetrier, D. Carlier, C. Masquelier, L. Croguennec, *J. Phys. Chem. C* **2017**, *121*, 4103.
[61] G. Kresse, J. Furthmller, *Comput. Mater. Sci.* **1996**, *6*, 15.
[62] G. Kresse, J. Furthmuller, *Phys. Rev. B* **1996**, *54*, 11169.
[63] G. Kresse, D. Joubert, *Phys. Rev. B* **1999**, *59*, 1758.
[64] P. E. Blochl, *Phys. Rev. B* **1994**, *50*, 17953.
[65] J. P. Perdew, K. Burke, M. Ernzerhof, *Phys. Rev. Lett.* **1996**, *77*, 3865.
[66] S. L. Dudarev, G. A. Botton, S. Y. Savrasov, C. J. Humphreys, A. P. Sutton, *Phys. Rev. B* **1998**, *57*, 1505.

